Stability and wave-vector restriction of axisymmetric Taylor vortex flow

Hermann Riecke and Hans-Georg Paap
Physikalisches Institut der Universität Bayreuth, D-8580 Bayreuth, Federal Republic of Germany
(Received 8 July 1985)

The stability of Taylor vortex flow with respect to axisymmetric perturbations is calculated numerically for several values of the radius ratio. In the nonlinear regime the resulting band of stable wave vectors is considerably smaller than predicted from amplitude expansions. On the low-q side the stability limit departs rather suddenly from the amplitude-expansion result with increasing reduced Reynolds number ε_R and is influenced by the appearance of two bifurcations, which are connected with the coupling of two flows with resonating wave vectors. The influence of these bifurcations becomes stronger with decreasing radius ratio. The wavelength-changing process, however, is still given by the Eckhaus mechanism. The numerical results are in very good agreement with recent quantitative experimental measurements.

I. INTRODUCTION

Many dissipative systems exhibit spontaneous pattern formation when some control parameter $\mathcal{R}$ is increased above a critical value $\mathcal{R}_c$. The two classical examples are Rayleigh-Bénard convection[1,2] and Taylor vortex flow.[3] In all of these systems the pattern has a uniquely defined wave vector q_c at threshold. Upon increasing $\mathcal{R}$ above $\mathcal{R}_c$, a continuous wave-vector band of stable solutions opens up. The limits of this band are given by a variety of instabilities, which in the case of Rayleigh-Bénard convection have been extensively studied both theoretically and experimentally.[4-6] For Taylor vortex flow (TVF) the theoretical stability limits with respect to axisymmetric perturbations have been determined so far only within the framework of amplitude expansions, which are valid close to threshold.[7-9] In the nonlinear regime these limits do not agree with recent high-precision measurements by Dominguez-Lerma *et al.*[10] Nonaxisymmetric perturbations have been considered in detail by Jones.[11-13] They do not simply restrict the band, but rather lead to other types of flow [wavy vortex flow (WVF), jet mode].[14,15]

The most important axisymmetric instability is the Eckhaus instability, which is *the* one-dimensional long-wavelength bulk instability.[16,17] It is present in most pattern-forming systems, but often it is superseded by others, which can be higher-dimensional bulk instabilities (e.g., zig-zag in Rayleigh-Bénard convection or nonaxisymmetric in TVF) or surface instabilities induced by boundaries. Roughly speaking, in order for the latter to be excluded the lateral boundaries may not lead to a depression of the pattern close to the sidewalls.[18-20]

So far, no detailed quantitative comparison between experimental and theoretical Eckhaus limits has been performed for any system. Semiquantitative agreement was found in the buckling instability of a rectangular plate.[21,22] In TVF the usually employed solid end plates provide boundary conditions that enhance the pattern via the Ekman vortex system. Also, nonaxisymmetric modes are only relevant for rather large values of $\varepsilon_R=(\mathcal{R}-\mathcal{R}_c)/\mathcal{R}_c$ if the ratio $\eta=R_1/R_2$ of the inner to the outer radius is chosen sufficiently below 1 (e.g., Ref. 23). Thus a comparison between experimental and theoretical stability limits is possible in the fully nonlinear regime.

We here present a numerical stability analysis of TVF with the outer cylinder at rest. Using a Galerkin procedure, axisymmetric solutions are calculated for three different values of η ($\eta=0.892, 0.75, 0.5$) and their stability with respect to axisymmetric perturbations is determined. It is found that for $\varepsilon_R>0.1$ the band of stable wave vectors is considerably smaller than that given by amplitude expansions to third order.[7,8] This is due to an interesting bifurcation structure involving flows with resonating wave vectors.[24] In addition, a fold appears at the low-q side of the band. The stability limit moves very close to the tip of this fold with increasing ε_R, but the band is still limited by the Eckhaus instability. When lowering η this behavior becomes more and more pronounced. The results agree very well with the data by Dominguez-Lerma *et al.*[10]

In Sec. II the basic equations are set up and the numerical procedures are described. The results are then presented in Sec. III. Concluding remarks are given in Sec. IV.

II. BASIC EQUATIONS AND NUMERICAL METHODS

To study axisymmetric solutions and perturbations to the Navier-Stokes equations for incompressible fluids, it is convenient to introduce a cylindrical polar coordinate system (r,ϕ,z) and a velocity potential ψ. The velocity field is then given by

$$\mathbf{u}(r,z)=(u_r,u_\phi,u_z)=\left[-\frac{1}{r}\frac{\partial\psi}{\partial z},u_\phi,\frac{1}{r}\frac{\partial\psi}{\partial r}\right]. \tag{2.1}$$

The basic flow (Couette flow) is purely azimuthal (see, e.g., Ref. 25),

$$u_\phi^0=\frac{\Omega_1 R_1}{1-\eta^2}\left[(1-\mu)\frac{R_1}{r}-(\eta^2-\mu)\frac{r}{R_1}\right], \tag{2.2}$$

where

$$\eta=R_1/R_2,\quad \mu=\Omega_2/\Omega_1\ , \tag{2.2a}$$

with $\Omega_{1,2}$ being the rotation rates of the inner and outer cylinder, respectively. (For generality, we allow Ω_2 to be arbitrary in this section.) We now introduce dimensionless variables $x,y,\bar{t},\bar{v},\bar{\psi}$ via

$$\begin{aligned} &x=zq/d,\quad y=2(r-R_1-d/2)/d,\quad \rho=r/R_2 \\ &\bar{t}=2\nu t/d^2,\quad \bar{v}=(u_\phi-u_\phi^0)/\Omega_1 R_1,\quad \bar{\psi}=\psi/\nu R_2\ , \end{aligned} \tag{2.3}$$

with q denoting the dimensionless wave vector of the periodic solution to be computed, d the gap width R_2-R_1, and ν the kinetic viscosity. With this scaling the azimuthal momentum equation and the azimuthal vorticity equation read, respectively (see, e.g., Ref. 11),

$$\begin{aligned} 2\rho\partial_t v=&\left[4\partial_y\rho\partial_y+q^2\rho\partial_x^2-(1-\eta)^2\frac{1}{\rho}\right]v \\ &-2q\frac{\eta^2-\mu}{\eta(1+\eta)}\partial_x\psi+(1-\eta)q\frac{1}{\rho}v\partial_x\psi-2q\frac{\partial(v,\psi)}{\partial(x,y)}\ , \end{aligned} \tag{2.4}$$

$$\begin{aligned} 2\rho\partial_t Z=&\left[4\partial_y\frac{1}{\rho}\partial_y\rho^2+q^2\rho\partial_x^2\right]Z \\ &+\mathcal{T}q\frac{\eta^3}{(\eta^2-\mu)(1-\eta)}\left[(1-\mu)\frac{1}{\rho^2}-\frac{\eta^2-\mu}{\eta^2}\right]\partial_x v \\ &+\mathcal{T}q\frac{\eta^2(1+\eta)}{\eta^2-\mu}\frac{1}{\rho}v\partial_x v+2q\frac{\partial(\psi,Z)}{\partial(x,y)}\ . \end{aligned} \tag{2.5}$$

Here overbars have been dropped. The Jacobian of a and b,

$$\frac{\partial(a,b)}{\partial(x,y)}=\frac{\partial a}{\partial x}\frac{\partial b}{\partial y}-\frac{\partial a}{\partial y}\frac{\partial b}{\partial x}\ , \tag{2.6}$$

the potential vorticity Z,

$$Z=-\left[\frac{4}{\rho}\partial_y\frac{1}{\rho}\partial_y+\frac{q^2}{\rho^2}\partial_x^2\right]\psi\ , \tag{2.7}$$

and the Taylor number $\mathcal{T}$,

$$\mathcal{T}=\frac{2\Omega_1^2 d^4(\eta^2-\mu)}{(1-\eta^2)\nu^2}\propto\mathcal{R}^2\ , \tag{2.8}$$

have been introduced.

The boundary conditions on the inner and the outer cylinder read

$$v=\psi=\partial_y\psi=0\ \text{ at } y=\pm1\ . \tag{2.9}$$

Here zero net flow along the cylinder has been assumed. Considering an infinite system, we use periodic boundary conditions in x direction.

The stability equations are given by the linearization of (2.4) and (2.5) around the nonlinear solution (v_0,ψ_0) and take the form

$$\underline{T}\partial_t\begin{pmatrix}v_1\\ \psi_1\end{pmatrix}=\underline{L}(v_0,\psi_0)\begin{pmatrix}v_1\\ \psi_1\end{pmatrix}\ , \tag{2.10}$$

where $\underline{T}$ and $\underline{L}(v_0,\psi_0)$ are linear operators and $\underline{L}$ depends on (v_0,ψ_0).

The nonlinear equations (2.4) and (2.5) are solved by use of a Galerkin method (see, e.g., Ref. 26). To this end we expand v and ψ in a combined (truncated) Fourier-Chebyshev series,

$$v=\sum_{k=-N}^{N}\sum_{m=0}^{M}\alpha_{m,k}T_m(y)\exp(ikx)\ , \tag{2.11}$$

$$\psi=\sum_{k=-N}^{N}\sum_{m=0}^{M}i\beta_{m,k}T_m(y)\exp(ikx)\ , \tag{2.12}$$

where

$$\alpha_{m,k}=\alpha^*_{m,-k},\quad \beta_{m,k}=-\beta^*_{m,-k}\ .$$

The cutoff parameter M can be chosen k dependent to render the expansion more efficient. Finite-difference calculations by Booz[27,28] show that well above threshold v can still be taken as even and ψ as odd in x. Therefore, one can choose $\alpha_{m,k}$ and $\beta_{m,k}$ to be real:

$$\alpha_{m,k}=\alpha_{m,-k},\quad \beta_{m,k}=-\beta_{m,-k}\ . \tag{2.13}$$

If this symmetry were broken at some point for a solution, which is connected to that at threshold, this would show up as an instability in the stability analysis. To get matrix equations for the coefficients $\alpha_{m,k}$ and $\beta_{m,k}$ we insert (2.11) and (2.12) into (2.4) and (2.5) and project the resulting equations onto

$$T_j(y)\exp(-ilx)(1-y^2)^{-1/2}\ .$$

This scalar product has been chosen to make use of the good boundary resolution of Chebyshev polynomials. In order to fulfill the radial boundary conditions (2.9), Lanczos's τ method is applied:[26] The v equation is projected only onto the first $M-2$, and the ψ equation onto the first $M-4$, Chebyshev polynomials for each Fourier mode l. The projections onto the highest 2 (4) Chebyshev modes are replaced by the $2+4$ boundary conditions (2.9). The resulting nonlinear algebraic equations are solved by Newton iteration.

For the axisymmetric perturbations (v_1,ψ_1) in (2.10) the Floquet *ansatz*

$$v_1=\sum_{k=-N}^{N}\sum_{m=0}^{M}\bar{\alpha}_{m,k}T_m(y)\exp(ikx)\exp(ipx+\sigma t)\ , \tag{2.14}$$

$$\psi_1=\sum_{k=-N}^{N}\sum_{m=0}^{M}i\bar{\beta}_{m,k}T_m(y)\exp(ikx)\exp(ipx+\sigma t) \tag{2.15}$$

is made. Since here no symmetry relation like (2.13) holds, the size of the matrices is doubled as compared to the previous ones. Applying the same Galerkin procedure as above, one is led to a generalized eigenvalue problem for the growth rate σ of the form

$$\underline{A}\mathbf{x}=\sigma\underline{B}\mathbf{x}\ , \tag{2.16}$$

where

$$\mathbf{x}=(\cdots\bar{\alpha}_{m,k}\cdots\bar{\beta}_{m,k}\cdots)\ .$$

The eigenvalue of interest is expected to be real, and the onset of instability is given by its sign change. A being nonsingular, the eigenvalue problem

TABLE I. Wave vectors of the tip of the fold (q_F) and of the Eckhaus limit (q_E) for different values of the cutoff parameter N in the Fourier expansion.

			$\varepsilon_R=1$				
	$\eta=0.75$				$\eta=0.5$		
M	N	q_F	q_E	M	N	q_F	q_E
12	5	2.29	2.321	12	5	2.716	2.720
12	7	2.23	2.261	12	7	2.61	2.620
12	9	2.22	2.254	12	9	2.60	2.607

$$\underline{A}^{-1}\underline{B}\mathbf{x}=\sigma^{-1}\mathbf{x} \tag{2.17}$$

can therefore be solved by inverse iteration.

The following comment appears in order: Numerical Galerkin procedures tend to very poorly reproduce eigenvalues for eigenvectors that are dominated by modes $T_m\exp(ikx)$ with m or k close to the cutoff parameters. In the problem at hand some of these (very large) eigenvalues have even the wrong sign, thus faking an instability which, in fact, is not present. For time-dependent studies this may lead to serious problems. Here it is of no consequence, as the relevant (small) eigenvalue is not affected for N and M large enough.

A criterion for the accuracy of the results is the change in the torque exerted on the cylinders, if the number of modes is increased. The torque on the outer cylinder (per unit length) is given by

$$G=\frac{2\bar{G}}{\eta^2}[\eta(1-\mu)/(1+\eta)-\langle\partial_y v(y=+1)\rangle]\ ,$$
$$\bar{G}=2\pi R_1^3\nu\rho'\Omega_1/d\ , \tag{2.18}$$

where $\langle\cdots\rangle$ denotes the average over x, and ρ' is the density of the fluid. A result was regarded to be satisfactory if the torque changed less than 1% when N was increased by 2. ($M=12$ turned out to be sufficient for all calculations.) Another test is given by the fact that σ must be an even periodic function in p with period 1. If not enough Fourier modes are retained, there will be strong deviations from this periodicity. The influence of N on the stability limit is demonstrated in Table I.

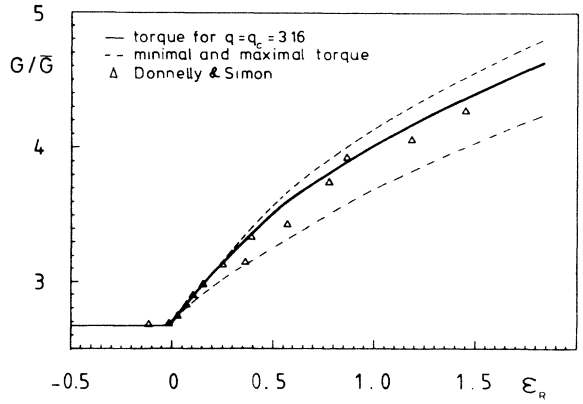

FIG. 1. Dimensionless torque $G/\bar{G}$ vs $\varepsilon_R\equiv(\mathscr{R}-\mathscr{R}_c)/\mathscr{R}_c$: numerical results for $q=3.16$ and spread due to the stable q band in comparison with experiments by Donnelly and Simon (Ref. 29).

III. NONLINEAR SOLUTIONS AND THEIR STABILITY

To check the quality of the nonlinear solutions obtained, it is conventional to compare the calculated torques with experimentally measured values. Like all of the physical quantities involved, the torque is not independent of the wave vector q of the flow. Therefore, a precise comparison of theory and experiment requires knowledge of both torque and wave vector. In Fig. 1 our results for the dimensionless torque $G/\bar{G}$ as a function of ε_R are compared with measurements by Donnelly and Simon[29] for radius ratio $\eta=0.5$ and $\mu=0$. As Donnelly and Simon do not give values for q, we show not only the torque for the critical wave vector $q_c=3.16$, but also indicate the spread of torques implied by the continuous band of stable wave vectors.

A comparison was also made with the numerical data for the torque and the radial velocity given by Jones.[30] Within his error bounds our data agree very well with his over the whole range $0\le\varepsilon_R\le 2$.

We have studied the stability of Taylor vortex flow with respect to axisymmetric perturbations in the case $\mu=0$ for three different values of the radius ratio: $\eta=0.892$, 0.75, and 0.5. In the first case, which corresponds to a small gap, one is limited to low values of $\varepsilon_R\equiv(\mathscr{R}-\mathscr{R}_c)\mathscr{R}_c$ as the transition to wavy vortex flow occurs already at $\varepsilon_R=0.12$.[31] The stability limits obtained in this case are shown in Fig. 2 (solid lines). As is to be expected close to threshold, the instability is of the Eckhaus type and the limits agree well with those given by third-order amplitude expansion[7] which are shown as dashed lines. The neutral curve is also given. Experiments for this radius ratio have been performed by Ahlers

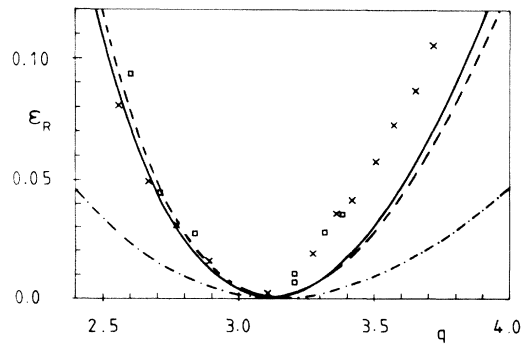

FIG. 2. Stability limits for $\eta=0.892$ [Eckhaus, ——; Eckhaus to third order, — — —; neutral curve, —·—·—·; experiments by Ahlers *et al.* (Ref. 31), □; and Dominguez-Lerma *et al.* (Ref. 10), ×].

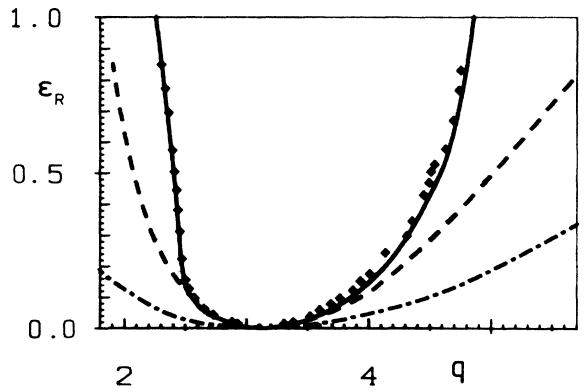

FIG. 3. Stability limits for $\eta=0.75$ [Eckhaus, ——; Eckhaus to third order, — — —; neutral curve, —·—·—·; experiments by Dominguez-Lerma *et al.* (Ref. 10), ◇].

et al.[31] and Dominguez-Lerma *et al.*,[10] who determined the stability limits by changing the aspect ratio of their apparatus. In Fig. 2 their data are given as squares and crosses, respectively. For $q>q_c$ they do not reach the theoretical Eckhaus curve, whereas for $q<q_c$ very good agreement is found.

Lowering η increases the range of ε_R for stable TVF considerably. At the same time the locus of the transition to WVF becomes strongly q dependent: Experiments by Cole[14] and calculations by Jones[13] show that for $\eta=0.75$ the transition to WVF occurs at $\varepsilon_R=1$ for $q=2.4$, whereas for $q=3.5$ it is delayed to $\varepsilon_R=5$. Axisymmetric perturbations are therefore expected to be dominant up to $\varepsilon_R=1$ and beyond, depending on q. The resulting stability limits for TVF are shown in Fig. 3 (solid line). Also given (as diamonds) are the experimental data by Dominguez-Lerma *et al.*,[10] who report that the instability occurs in the bulk and is axisymmetric. It is seen that the theoretical results reproduce the data very well over the whole relevant range of Reynolds numbers. This constitutes the first detailed, quantitative agreement of theoretical and experimental Eckhaus limits. For comparison the stability limits as determined by the amplitude expansion (dashes) and the neutral curve (dashed-dotted) are also given. As expected, the former gives good results close to threshold ($\varepsilon_R<0.1$). For larger ε_R the expansion does very poorly, especially on the low-q side, where it fails to reproduce the strong bend at $q=2.5$. The numerical analysis reveals that this bend is not due to a change in the type of the instability: It is still of the Eckhaus type ($p\to 0$). Instead, the solutions themselves change their character and two bifurcations, which are discussed below, show up. This bifurcation structure has been studied in some detail by several authors.[32,33,12,24,34] They did not, however, study the stability of the solutions obtained. Quantitative predictions for the observable band of wave vectors were therefore not possible.

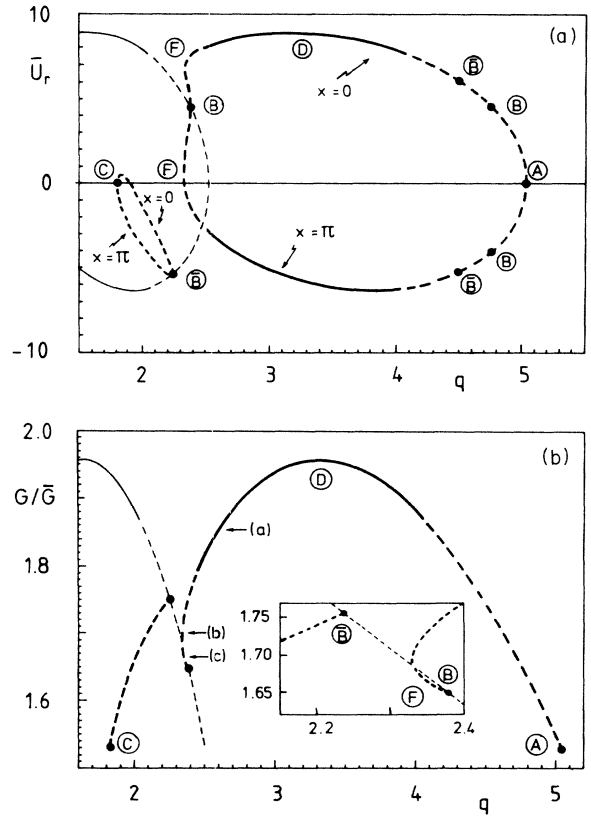

FIG. 4. (a) Bifurcation diagram in terms of the radial velocity $\bar{u}_r$ at $x=\pi$ and $x=0$ for $\eta=0.75$ and $\varepsilon_R=0.195$ (stable, ——; unstable, — — —). For details see the text. (b) Bifurcation diagram in terms of the dimensionless torque $G/\bar{G}$ for $\eta=0.75$ and $\varepsilon_R=0.195$ (stable, ——; unstable, — — —). For details see the text. The arrows indicate wave vectors for which solutions are shown in Figs. 5(a)–5(c).

To better understand the following it is useful to recognize that any 2π-periodic flow (one vortex pair per wavelength $2\pi/q$) of wave vector q can also be looked at as being π periodic (two vortex pairs per wavelength) with wave vector $q/2$. Thus, the neutral curve can be represented either as the neutral curve for 2π-periodic flow centered around q_c or as that of the π-periodic flow centered around $q_c/2$. Above the intersection point of the two curves, 2π-periodic solutions as well as π-periodic solutions exist for the same (small) value of q. For the range $0.5\le\eta\le 1$ this occurs for $\varepsilon_R>0.1$. As the nonlinearity of the hydrodynamic equations is quadratic, these two modes interact. For increasing ε_R this interaction becomes stronger and leads to the bifurcation diagrams shown in Figs. 4(a) and 4(b) (for $\varepsilon_R=0.195$). Figure 4(a) shows the dimensionless radial velocity $\bar{u}_R=u_r d/\nu$ for the same flow at $x=0$ and $x=\pi$ as a function of q, similar to Fig. 4 of Meyer-Spasche and Keller.[24] The chosen values of x correspond for the 2π-periodic flow around D to the location of maximal outward and inward velocity, respectively. Figure 4(b) displays the same bifurcation structure in terms of the dimensionless torque $G/\bar{G}$. In order to display the connectedness of the structure, in both figures each value is plotted for the 2π-periodic (heavy lines) as well as the π-periodic flow (thin lines).

Starting in the stable regime at D (solid lines, stable; dashed lines, unstable), one reaches the neutral curve at A by continuously increasing the wave vector. Decreasing q, however, one does not reach the neutral curve. Instead, one ends up at the fold F ($q=2.33$). This fold is connect-

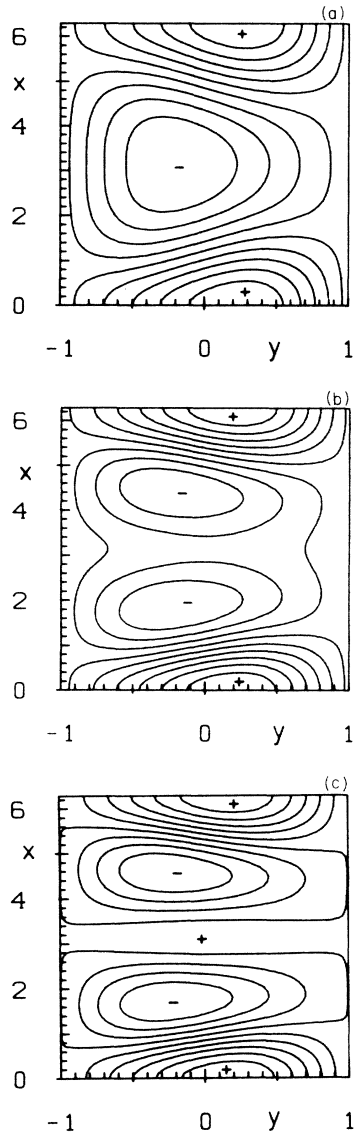

FIG. 5. Contours of equal azimuthal velocity v for $\eta=0.75$ and $\varepsilon_R=0.195$ [(a) $q=2.6$, (b) $q=2.33$, and (c) $q=2.35$] [cf. Fig. 4(b)].

ed to the bifurcation point B ($q=2.38$), where the flow becomes π periodic and is thus identical to the one at $2q=4.76$ [$\bar{u}_r(x=0)=\bar{u}_r(x=\pi)$]. Analogously, the 2π-periodic flow starting from the left neutral curve at C turns into a π-periodic flow at the bifurcation point $\bar{B}$ ($q=2.25$). Thus, along both branches additional vortices are being built in continuously, as is displayed in Figs. 5(a)–5(c). Here contour lines of the azimuthal velocity component v of the flow are shown for three values of q, which are indicated by arrows in Fig. 4(b). Note that for q values in the (small) gap between $\bar{B}$ and F there exists no solution with primitive period 2π. Figures 4(a) and 4(b) show also that the bifurcation diagram alone does not suffice to determine the stability and the resulting wave-vector band of TVF. Neither the fold nor the bifurcation points coincide with the stability limits. On the other hand, it is clear that the strong q dependence of the flow close to the fold has a pronounced effect on the instability: Its onset becomes very sudden for larger Reynolds numbers—a small decrease of q leads to a large increase of the growth rate σ—and is shifted closer to the tip of the fold, which becomes rather prominent [cf. Table I in comparison with Figs. 4(a) and 4(b)]. This may account for the remarkably good agreement between theoretical and experimental stability limits.

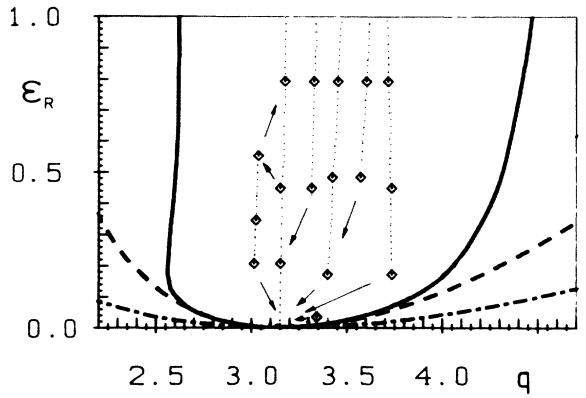

FIG. 6. Stability limits for $\eta=0.5$ [Eckhaus, ——; Eckhaus to third order, — — —; neutral curve, —·—·—·; experiments by Snyder (Ref. 23), ◇]. (See the text.)

Decreasing the radius ratio to $\eta=0.5$ further enhances the deviations from the third-order theory (for $\varepsilon_R>0.1$), as can be seen in Fig. 6 (solid line, numerical analysis; dashed line, third-order theory). At the same time, the wave-vector band becomes strikingly asymmetric. This is due to the increased importance of the π-periodic flow for $q<q_c$ as compared to the case $\eta=0.75$, as is illustrated in Table I: It gives the wave vectors q_F and q_E corresponding to the tip of the fold and the stability limit, respectively, for three values of N, the number of Fourier modes retained. Clearly the convergence in N is slower for $\eta=0.5$. Table I also demonstrates that the stability limit moves closer to the tip of the fold with decreasing η. The importance of these interactions also becomes clear when comparing the results with the stability limits obtained by Nakaya using a fifth-order amplitude theory.[9,35] For $q>q_c$ it gives good results for a larger ε_R interval than

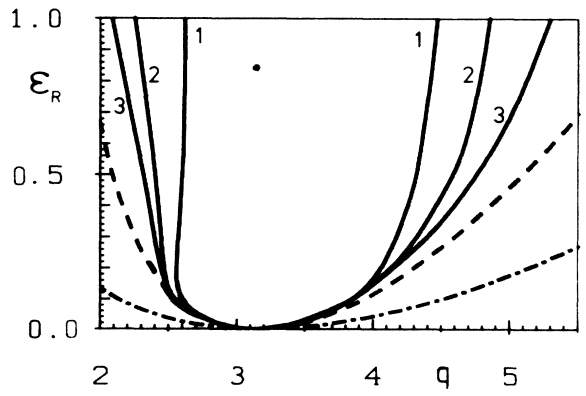

FIG. 7. Comparison of the stability limits for $\eta=0.5$ (curve 1), $\eta=0.75$ (curve 2), and $\eta=0.892$ (curve 3) (Eckhaus to third order, — — —; neutral curve, —·—·—·; both are almost independent of η). Note that for $\eta=0.892$ TVF is unstable to nonaxisymmetric perturbations for $\varepsilon_R>0.12$.

the third-order theory. Yet, it still misses the strong bend at $q=2.6$ completely, indicating that at least two independent modes are necessary to describe the flow in that region. Included in Fig. 6 are the only experimental data available for this radius ratio, which were given by Snyder,[23] who looked at the transitions between different numbers of vortices after changes in the Reynolds number, rather than changing the wave vector continuously with ε_R fixed. States with the same number of vortices are connected by dots, transitions are marked by arrows. Clearly his experimental procedure does not give the full band.

To give an overview of the dependence of the stable band on the radius ratio, Fig. 7 shows the stability limits for all three values of η (solid lines). Again the neutral curve (short and long dashes) and the Eckhaus limit to third order (dashed line), which are almost independent of η, are also given.

IV. CONCLUDING REMARKS

The kind of interaction, which in Sec. III was seen to be responsible for the asymmetrical narrowing of the stable wave-vector band, is present in all pattern-forming systems, if the control parameter is chosen large enough to yield a sufficiently wide neutral curve. In most systems, however, this has no influence on the stability limits, as the bifurcations and folds, if any, appear only far out in the unstable regime (compare, e.g., Fig. 9 of Ref. 36 with our Table I). It appears to be a peculiarity of the wide-gap TVF to react so sensitively to these interactions. For $q>q_c$ the bifurcation structure appears to have no influence on the stability limits for $\varepsilon_R \leq 1$ and $\eta \geq 0.5$.

A direct consequence of the bifurcation structure is that the longitudinal phase diffusion constant $D_{||}$ diverges at the fold due to terms involving derivatives with respect to q (see, e.g., Refs. 37 and 38). The stability limit will therefore never coincide with the tip of the fold. In contrast to the high-q side,where the divergence occurs only on the neutral curve, this divergence is well within the neutral band, and for $\varepsilon_R \geq 0.5$ it occurs very close to the stability limit. Thus, the q dependence of $D_{||}$ near the low-q band edge is much stronger than that on the high-q side. By now, experiments allow measurement of the phase diffusion constant quantitatively.[39] Therefore, it should be possible to verify this aspect of the bifurcation structure experimentally.

As the interaction becomes stronger with increasing ε_R and decreasing η, it would be interesting to do experiments for $\eta=0.5$—which could check our numerical findings—or even smaller values of η. For these radius ratios TVF is stable with respect to nonaxisymmetric perturbations up to $\varepsilon_R=3$ and beyond. Thus, it allows us to study the aforementioned interactions and the stability limits for even stronger nonlinearity. Numerical work in that direction ($\varepsilon_R>1$, $\eta \leq 0.5$) is in progress.

ACKNOWLEDGEMENTS

The authors gratefully acknowledge helpful discussions with R. M. Clever, L. Kramer, and F. H. Busse, and also wish to thank L. Kramer and F. H. Busse for critically reading the manuscript. We also wish to thank C. A. Jones for sending us reports of his work (Refs. 13 and 30) prior to publication, and especially G. Ahlers for making experimental data of Ref. 10 available to us at an early stage.

[1]C. Normand, Y. Pomeau, and M. G. Velarde, Rev. Mod. Phys. **49**, 581 (1977).
[2]F. H. Busse, Rep. Prog. Phys. **41**, 1929 (1978).
[3]R. C. DiPrima and H. L. Swinney in *Hydrodynamic Instabilities and the Transition to Turbulence,* edited by H. L. Swinney and J. P. Gollub (Springer, Berlin, 1981).
[4]F. H. Busse and J. A. Whitehead, J. Fluid Mech. **47**, 305 (1971).
[5]F. H. Busse and R. M. Clever, J. Fluid Mech. **91**, 319 (1979).
[6]A. Pocheau and V. Croquette, J. Phys. (Paris) **45**, 35 (1984).
[7]S. Kogelman and R. C. DiPrima, Phys. Fluids **13**, 1 (1970).
[8]F. H. Busse, in *Instability of Continuous Systems,* edited by H. Leipholz (Springer, Berlin, 1971).
[9]C. Nakaya, J. Phys. Soc. Jpn. **36**, 1164 (1974).
[10]M. A. Dominguez-Lerma, D. Cannell, and G. Ahlers (private communication), and unpublished.
[11]C. A. Jones, J. Fluid Mech. **102**, 249 (1981).
[12]C. A. Jones, J. Fluid Mech. **120**, 433 (1982).
[13]C. A. Jones, J. Fluid Mech. **157**, 135 (1985).
[14]J. A. Cole, in Proceedings of the Third Taylor Vortex Flow Working Party, Nancy, 1983 (unpublished).
[15]A. Lorenzen, G. Pfister, and T. Mullin, Phys. Fluids **26**, 10 (1983).
[16]W. Eckhaus, *Studies in Nonlinear Stability Theory* (Springer, New York, 1965).
[17]L. Kramer and W. Zimmerman, Physica **16D**, 221 (1985).
[18]M. C. Cross, P. G. Daniels, P. C. Hohenberg, and E. D. Siggia, J. Fluid Mech. **127**, 155 (1983).
[19]L. Kramer and P. C. Hohenberg, Physica **13D**, 357 (1984).
[20]P. C. Hohenberg, L. Kramer, and H. Riecke, Physica **15D**, 402 (1985).
[21]W. Zimmermann and L. Kramer, J. Phys. (Paris) **46**, 343 (1985).
[22]M. Boucif, J. E. Wesfreid, and E. Guyon, J. Phys. (Paris) Lett. **45**, L413 (1984).
[23]H. A. Snyder, J. Fluid Mech. **35**, 273 (1969).
[24]R. Meyer-Spasche and H. B. Keller, Phys. Fluids **28**, 1248 (1985).
[25]L. D. Landau and E. M. Lifschitz, *Hydrodynamik,* Band 6 of *Lehrbuch der theoretischen Physik* (Akademie, Berlin, 1974).
[26]C. A. J. Fletcher, *Computational Galerkin Methods* (Springer, New York, 1984).
[27]O. Booz, Ph.D. thesis, Institut A für Mechanik der Universität Stuttgart, 1980.
[28]H. Fasel and O. Booz, J. Fluid Mech. **138**, 21 (1984).
[29]R. J. Donnelly and N. J. Simon, J. Fluid Mech. **7**, 401 (1960).
[30]C. A. Jones, J. Comp. Physics (to be published).
[31]G. Ahlers, D. S. Cannell, and M. A. Dominguez-Lerma, Phys. Rev. A **27**, 1225 (1983).
[32]J. P. Andreichikov, Izv. Akad. Nauk SSR, Mekh. Zhidk.

Gaza No. 1, 47 (1977).
[33]G. Frank and R. Meyer-Spasche, J. Appl. Math. Phys. (ZAMP) **32**, 710 (1981).
[34]R. Meyer-Spasche and H. B. Keller (unpublished).
[35]His data are not shown, as his Fig. 4 does not allow a *quantitative* comparison with present results.
[36]M. Nagata and F. H. Busse, J. Fluid Mech. **135**, 1 (1983).
[37]L. Kramer, E. Ben-Jacob, H. Brand, and M. C. Cross, Phys. Rev. Lett. **49**, 1891 (1982).
[38]L. Kramer and H. Riecke, Z. Phys. B **59**, 245 (1985).
[39]G. Pfister (private communication).